

PL-TR-94-2164

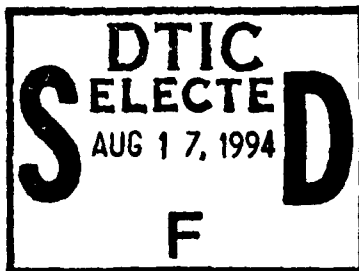
AD-A283 304



(2)

**CHEMICAL KINETICS AND
ATMOSPHERIC MODIFICATION**

David L. McFadden



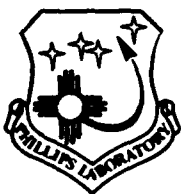
Boston College
140 Commonwealth Avenue
Chestnut Hill, MA 02167

1 May 1994

Final Report
31 August 1989-31 December 1993

approved for public release; distribution unlimited

2596 94-25964



PHILLIPS LABORATORY
Directorate of Geophysics
AIR FORCE MATERIEL COMMAND
HANSCOM AIR FORCE BASE, MA 01731-3010

94 8 10 142

"This technical report has been reviewed and is approved for publication"


ALBERT A. VIGGIANO
Contract Manager


JOHN F. PAULSON
Branch Chief


WILLIAM K. VICKERY
Division Director

This report has been reviewed by the ESC Public Affairs Office (PA) and is releasable to the National Technical Information Service (NTIS).

Qualified requestors may obtain additional copies from the Defense Technical Information Center (DTIC). All others should apply to the National Technical Information Service (NTIS).

If your address has changed, if you wish to be removed from the mailing list, or if the addressee is no longer employed by your organization, please notify PL/TSI, 29 Randolph Road, Hanscom AFB, MA 01731-3010. This will assist us in maintaining a current mailing list.

Do not return copies of this report unless contractual obligations or notices on a specific document requires that it be returned.

REPORT DOCUMENTATION PAGE

Form Approved
OMB No. 0704-0188

Public reporting burden for this collection of information is estimated to average 1 hour per response, including the time for reviewing instructions, searching existing data sources, gathering and maintaining the data needed, and completing and reviewing the collection of information. Send comments regarding this burden estimate or any other aspect of this collection of information, including suggestions for reducing this burden, to Washington Headquarters Services, Directorate for Information Operations and Reports, 1215 Jefferson Davis Highway, Suite 1204, Arlington, VA 22202-4302, and to the Office of Management and Budget, Paperwork Reduction Project (0704-0188), Washington, DC 20503.

1. AGENCY USE ONLY (Leave blank)		2. REPORT DATE 1 May 1994	3. REPORT TYPE AND DATES COVERED Final (31 Aug 1989-31 Dec 1993)	
4. TITLE AND SUBTITLE Chemical Kinetics and Atmospheric Modification			5. FUNDING NUMBERS PE 62101F PR 627A TA BM WU XX	
6. AUTHOR(S) David L. McFadden			Contract F19628-89-K -0043	
7. PERFORMING ORGANIZATION NAME(S) AND ADDRESS(ES) Boston College 140 Commonwealth Avenue Chestnut Hill, MA 02167			8. PERFORMING ORGANIZATION REPORT NUMBER	
9. SPONSORING/MONITORING AGENCY NAME(S) AND ADDRESS(ES) Phillips Laboratory 29 Randolph Road Hanscom AFB, MA 01731-3010 Contract Manager: Albert Viggiano/GPID			10. SPONSORING/MONITORING AGENCY REPORT NUMBER PL-TR-94-2164	
11. SUPPLEMENTARY NOTES				
12a. DISTRIBUTION / AVAILABILITY STATEMENT Approved for public release; Distribution unlimited			12b. DISTRIBUTION CODE	
13. ABSTRACT (Maximum 200 words) Electron attachment rate constants were obtained and negative ion product analysis was performed over the temperature range $300 \leq T(K) < 1200$ for a series of seventeen halomethane molecules that undergo dissociative electron attachment. The reactant molecules include CH_3Cl , CH_3Br , CH_3I , CF_3Cl , CF_3Br , CF_3I , CF_2Cl_2 , $CFCl_3$, CCl_4 , CF_3H , CF_2H_2 , CH_3F , CF_2HCl , $CHFCl_2$, CH_2Br_2 , CCl_2H_2 , and CCl_3H . Positive activation energies were observed for most of the reactions. The results of molecular structure calculations for both the neutral and anionic species suggest that the magnitude of the rate constants and of the temperature coefficients for dissociative electron attachment in these systems can be understood in terms of the geometrical reorganization associated with negative ion formation.				
14. SUBJECT TERMS Chemical kinetics Electron attachment Free radical reactions		Flow Tube Electron cyclotron resonance Photoionization mass spectro- metry		15. NUMBER OF PAGES 36
				16. PRICE CODE
17. SECURITY CLASSIFICATION OF REPORT Unclassified	18. SECURITY CLASSIFICATION OF THIS PAGE Unclassified	19. SECURITY CLASSIFICATION OF ABSTRACT Unclassified	20. LIMITATION OF ABSTRACT SAR	

CONTENTS

1.	Introduction	1
2.	Description of the Experiments	2
2.1	Flow Tube, EPR Cavity, Mass Spectrometer	2
2.2	Production of Free Electrons	6
2.3	Reactant Gas Delivery System and Reactant Inlet	7
2.4	Measurements	7
3.	Experimental Results	8
4.	Theoretical Model for Temperature Dependent Rate Constants	17
4.1	Calculations	22
4.2	Results and Discussion	27
	References	31

Accession For	
NTIS CRA&I	<input checked="" type="checkbox"/>
DTIC TAB	<input type="checkbox"/>
Unannounced	<input type="checkbox"/>
Justification	
By	
Distribution /	
Availability Codes	
Dist	Avail and/or Special
A-1	

1. Introduction

Electron-molecule interactions at high temperature play an important role in atmospheric plasmas. For example, an understanding of the kinetics of electron attachment reactions is fundamental to the development of plasma modification methods for altering radar signatures or for eliminating communication blackouts caused by plasma interference, to name two important applications. The aim of the research performed at Boston College and described in this report was a systematic study of electron attachment processes over a broad temperature range with the goal of understanding and ultimately of predicting the temperature dependence for dissociative electron attachment at thermal energies.

In the 1970's, Schulz and Spence [1] obtained the temperature dependence of the total cross section for the dissociative attachment of low energy electrons to seven halocarbon compounds. The results indicated a positive temperature dependence for this type of reaction for most of the halocarbons studied. All of the reactions that were studied are exoergic, and no energy barrier is expected for formation of the anionic intermediates. The reasons for the observed wide range of room temperature rates as well as for the observed positive temperature dependence were not elucidated. Our work was undertaken to extend the results of Schulz et al., to establish a larger kinetics data base that would serve as a basis for modeling dissociative electron attachment reactions, and to attempt the development of a predictive model for this class of reactions.

In the present experiments electron attachment rate constants were obtained and negative ion product analysis was performed over the temperature range $300 \leq T(K) \leq 1200$ for a series of seventeen halomethane molecules that undergo dissociative electron attachment. The reactant molecules include CH_3Cl , CH_3Br , CH_3I , CF_3Cl , CF_3Br , CF_3I , CF_2Cl_2 , CFCl_3 , CCl_4 , CF_3H , CF_2H_2 , CH_3F , CF_2HCl , CHFCl_2 , CH_2Br_2 , CCl_2H_2 and CCl_3H . Positive activation energies were observed for most of the reactions. The results of molecular structure calculations for both the neutral and anionic species suggest that the magnitude of the rate constants and of the temperature coefficients for dissociative electron attachment in these systems can be understood in terms of the geometrical reorganization associated with negative ion formation.

The experiments are described in Section 2. The experimental results are presented in Section 3. Model calculations for predicting the temperature dependent rate constant for dissociative electron attachment are presented in Section 4. The model, which is based on changes in bond length that accompany electron attachment provides some, but not complete, agreement with the experimental data.

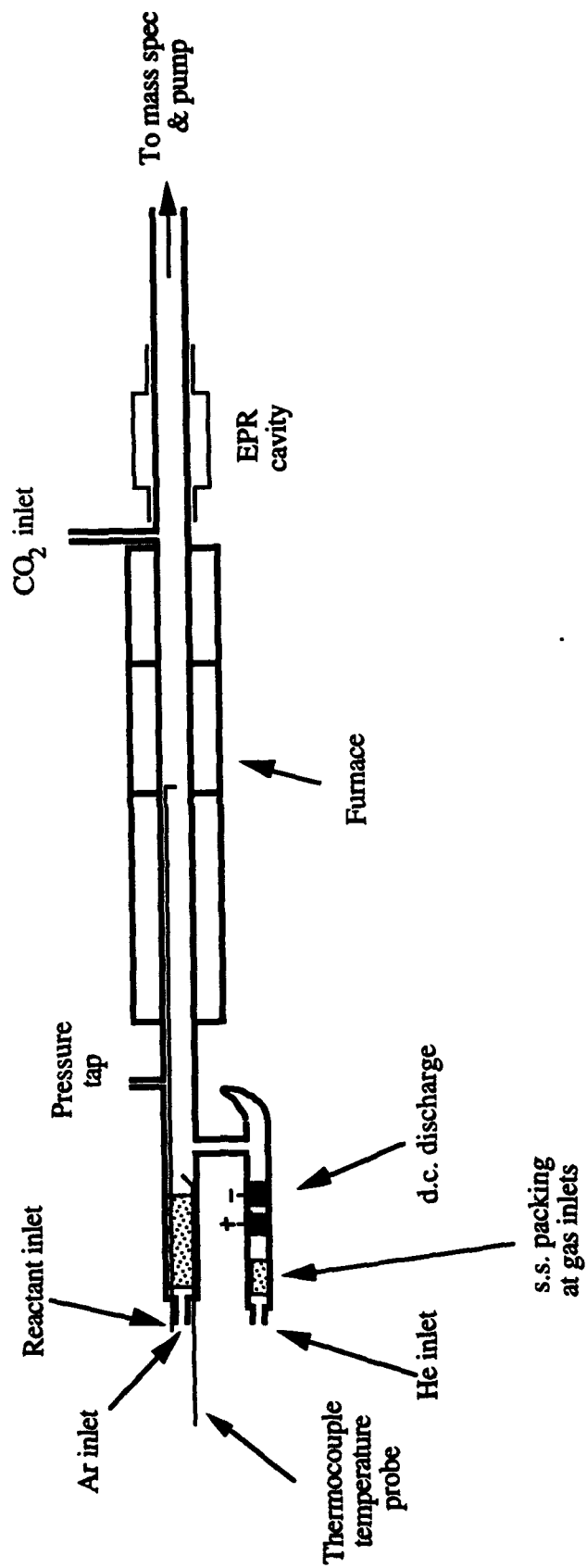
2. Description of the Experiments

The experiments are performed in a heated quartz, discharge-flow system. Thermal energy electrons are produced by Penning ionization of argon by metastable helium atoms, mixed with molecular reactants in a heated section of the flow tube, and detected by electron cyclotron resonance (ECR) absorption in a commercial electron paramagnetic resonance (EPR) spectrometer. The flow system is coupled to a quadrupole mass spectrometer for analysis of negative ion products.

2.1. Flow Tube, EPR Cavity, Mass Spectrometer

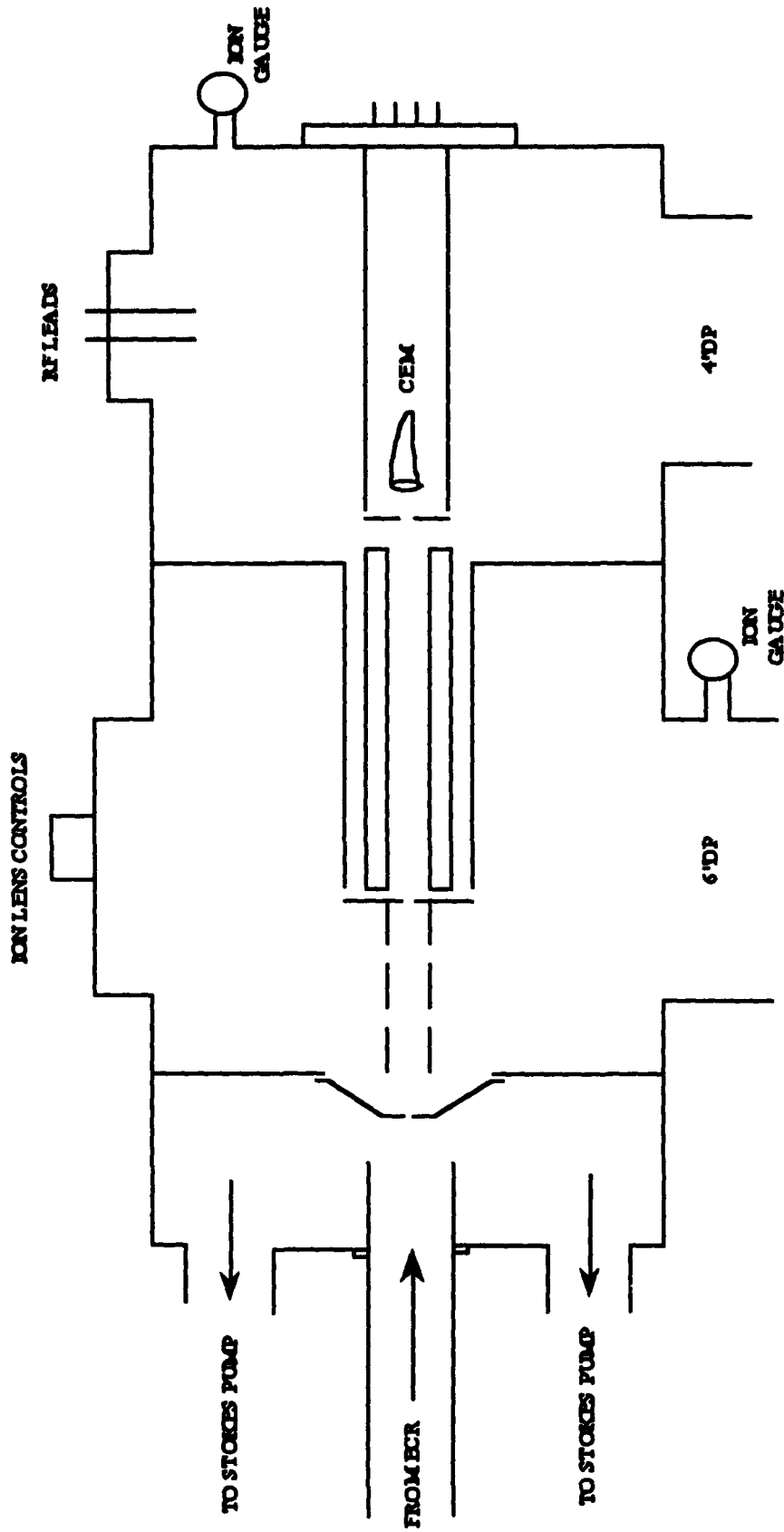
The experimental apparatus is shown in Figures 1 and 2. The main flow tube is made of 32 mm i.d. \times 35 mm o.d. quartz tubing and the side arm is made of 23 mm i.d. \times 25 mm o.d. quartz tubing. The side arm is attached to a Wood's horn to prevent photons created in the dc discharge from reaching the main flow tube.

The reaction zone is heated with four six-inch sections of clam shell ceramic heaters (Mellen Corp.), 24 inches long. The furnace is insulated by a 1 inch thick alumina blanket (Zircar Corp.) and powered by a direct current power supply (150 V, 50 A; Oriel Optics Corp.). The axial and radial temperature profiles in the reaction zone under experimental flow conditions are measured by using a movable thermocouple probe. The furnace is operated continuously on a 24 hour basis. Temperature profiles of the heated zone are shown in Figure 3.



Heated Discharge-Flow/Electron Cyclotron Resonance Apparatus

Figure 1



NEGATIVE ION QUADRUPOLE MASS SPECTROMETER

Figure 2

TYPICAL TEMPERATURE PROFILES IN THE REACTION ZONE

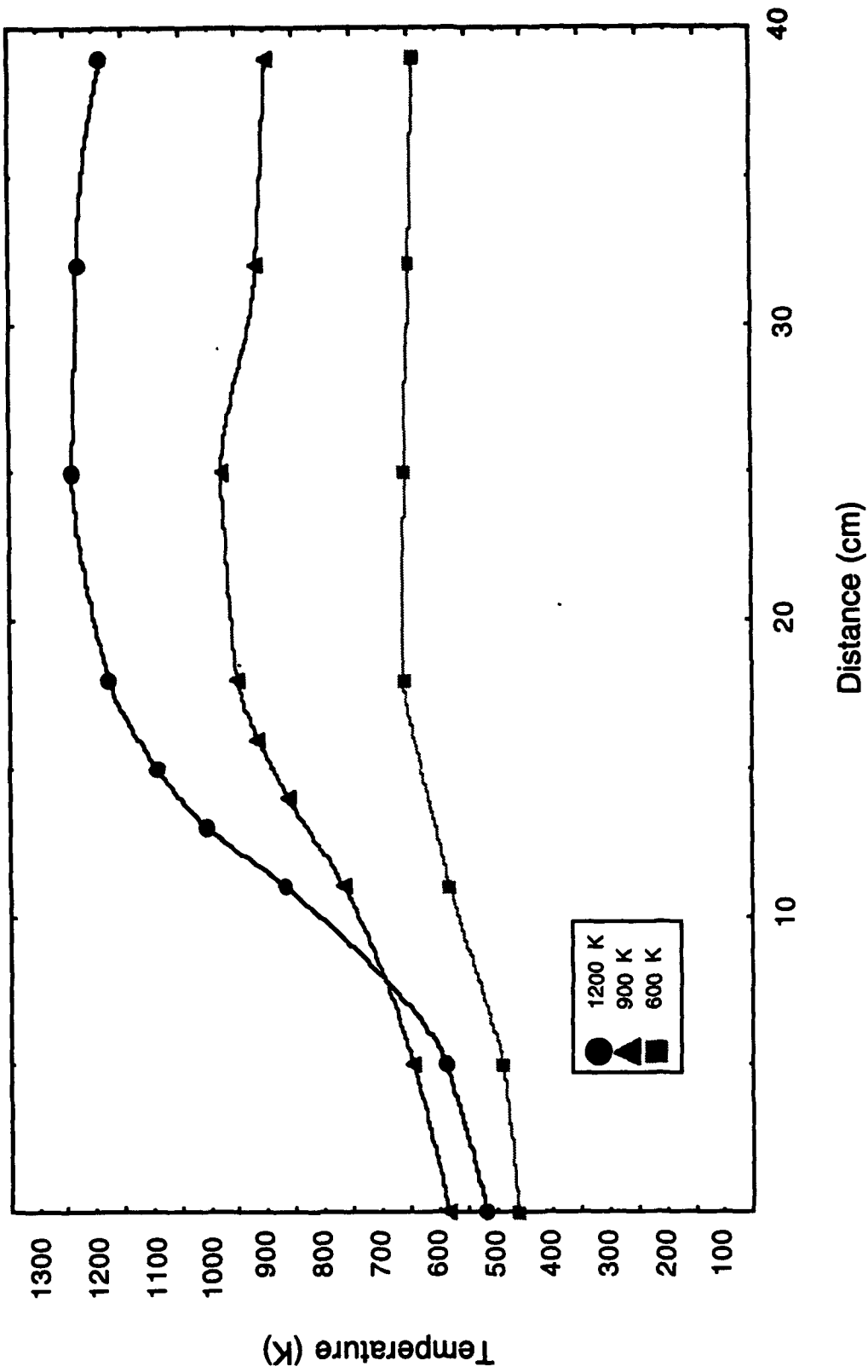


Figure 3

After passing through the reaction zone, electrons are detected by electron cyclotron resonance (ECR) absorption. In order to insure that the electrons are not heated by microwave absorption in the electron paramagnetic resonance (EPR) cavity, carbon dioxide is introduced as a thermalizing gas through an inlet located just before the cavity.

The EPR cavity is a large access cavity (Varian E-235) which employs 100 kHz magnetic field modulation and phase sensitive detection. The X-band klystron is typically operated at 0.02 mW of output power. The magnetic field is supplied by a 9 inch electromagnet (Varian V-3400), which has a 7 kW power supply.

Negative ion product analysis is performed downstream in a quadrupole mass spectrometer shown in Figure 2.

The flow tube is evacuated during experiments by a Stokes Microvac 212-H11 150 CFM (cubic feet per minute) rotary pump. Overnight, the entire system is evacuated by a Welch Duo-seal 1400 pump, which has a 0.9 CFM capacity. It typically keeps the system pressure at 25-30 microns. During experiments this pump is isolated from the system by a Worcester ball valve.

2.2. Production of Free Electrons

Electrons are produced by Penning Ionization of argon by helium metastable atoms produced in a DC discharge. The DC discharge is located in a sidearm connected to the main flow tube at a 90° angle. Ultra-pure helium (Wesco grade 4.7) is introduced into the system via 1/4 inch copper tubing. Before entering the sidearm and passing through the DC discharge, the helium is further purified in a liquid nitrogen cooled trap containing activated molecular sieves (Linde, types 5A and 13X). The voltage drop across the discharge, maintained by a Heath High Voltage Supply Model #SP-2717-A, is 200-270 Volts, depending on the pressure of the flow tube. A 0.1 megohm resistor in the circuit is found to optimize the electron signal and to give a 10-15 mA current in the discharge. After being formed in the discharge, helium metastable atoms travel downstream to the main flow tube.

Research grade argon is introduced into the main flow tube via 1/4 inch copper tubing upstream of the sidearm. The argon reacts with the helium metastable atoms to produce free electrons at the location where the sidearm is joined to the main flow tube.

2.3. Reactant Gas Delivery System and Reactant Inlet

The flow rates of reactant gases are determined by measuring the rate of pressure drop in a calibrated volume by using a differential capacitance manometer (MKS Baratron Model 221A). Dilute mixtures of most reactants are required in order to deliver reactant flow rates as low as 2×10^{-5} sccm. Helium is used as the diluent gas, and compositions range from 0.02 to 100%, depending on the reaction rate. The reactant gas flow can either be directed to the reactant inlet or to a "dump" line. Thus reactant on-off measurements can be made without disturbing the small flows once they are established. A small amount (about 10 sccm) of the total argon flow rate is diverted through the reactant inlet both to aid mixing of the reactant with the main flow and to maintain a constant flow through the reactant inlet when the reactant flow is switched on and off. Total pressure in the flow board is measured with an MKS 222CA 0-1000 Torr capacitance manometer.

Reactant gases are added through a movable inlet made of 1/4 inch fused quartz tubing. The inlet rests on the bottom of the flow tube and has a ring at the end that is bent up at a 90° angle to the flow tube. The ring has 6 small holes facing upstream through which the reactant gas is introduced into the main flow tube. The inlet position is fixed during the experiment and the reactant gas concentration is varied.

2.4. Measurements

A relative rate method is employed to determine the electron attachment rate constants with SF₆ as the reference standard. For fixed reactant inlet position and identical temperature profile and flow conditions, two sets of measurements of the ratio of electron concentration with and without reactant gas added, $[e^-]_{on}/[e^-]_{off}$, are taken as a function of reactant concentration, one set for the reference compound, SF₆, and another for the compound of interest. A semilog plot of

electron attenuation, $[e^-]_{on}/[e^-]_{off}$, versus reactant concentration yields a slope that is proportional to the rate constant. The ratio of slopes for the two compounds gives the ratio of rate constants. The electron attachment rate constant for SF₆ is assumed to be constant over the temperature range of the experiments. A value of $2.2 \times 10^{-7} \text{ cm}^3 \text{ s}^{-1}$ was assumed for the rate constant. Crompton et al. measured the same rate constant at 293 and 500 K for SF₆[2]. Schulz et al. measured the energy integrated cross section for electron attachment up to 1500 K and found it to be temperature independent.[1]

The product negative ion mass spectrum for each compound is recorded to identify the major product ion(s) that result from electron attachment.

3. Results

Typical examples of the kinetics measurements are shown in Figures 4-6 (pp. 10-12). A summary of the bimolecular rate constants derived from the slopes of these and similar plots is presented in Table 1 (p. 9). Five of the compounds listed in the table presented serious problems. These included CH₃Cl, CH₃F, CH₂F₂, CHF₃, and CHF₂Cl. Based on positive enthalpy changes calculated for their reactions, CH₃F, CH₂F₂ and CHF₃ were not expected to undergo dissociative electron attachment. The value of ΔH for the CHFCl₂ reaction may also be slightly positive. CHF₃, CH₂F₂ and CF₂HCl gave the appearance of reacting normally, albeit slowly, at room temperature. There was nothing unusual about the room temperature measurements, but at elevated temperature, the semilog plots of electron attenuation versus reactant concentration for all five compounds were highly curved as shown, for example, in Figure 7 (p. 13). It is possible that the small room temperature reaction rate could be due to the presence of an impurity in the reactant gas, since large reactant concentrations are required to observe the slowest reactions. However, we do not have a satisfactory explanation for the apparent fall-off in rate with increasing reactant concentration that is evident in Figure 7. Also we cannot explain why the data are again well behaved and show no curvature at 932 K for the two molecules investigated to date. Further work on these molecules is necessary.

There also appeared to be a problem with thermal decomposition of CF₃I and CF₃Br at the highest temperatures. The rate constants for CF₃I and CF₃Br showed a positive temperature dependence below 1000 K, but they turned over and fell at the highest temperature, which was taken as evidence of thermal decomposition as noted in the table.

Table 1. Rate constants, k_p ($\text{cm}^3 \text{ molecule}^{-1} \text{ s}^{-1}$), for thermal electron attachment reactions as a function of temperature.

Compound	Temperature (K)					
	293	467	615	579	932	1022
	k(T) ($\text{cm}^3 \cdot \text{sec}^{-1}$)					
CH ₃ I	1.00E-07			1.21E-07		
CH ₃ Br	5.95E-12		8.30E-10		9.48E-09	1.39E-08
CH ₃ Cl	too slow to meas.	curvature in data		curvature in data	5.09E-10	8.38E-10
CF ₃ I	2.20E-07		2.36E-07		2.23E-07	decomposes
CF ₃ Br	1.24E-08		3.89E-08		1.17E-07	decomposes
CF ₃ Cl	4.17E-13	1.32E-11		2.42E-10	9.50E-10	6.29E-09
CF ₂ Cl ₂	1.88E-09	1.38E-08		2.42E-08	3.91E-08	
CFCl ₃	2.36E-07	1.80E-07		2.10E-07		
CCl ₄	3.60E-07	1.26E-07		1.37E-07		
POCl ₃	8.00E-08			4.64E-08		
CF ₃ H	4.31E-13	curvature in data		curvature in data		
CF ₂ H ₂	2.75E-13	curvature in data		curvature in data		
CH ₃ F	too slow to meas.	curvature in data		curvature in data		
CF ₂ HCl	1.22E-13	curvature in data		curvature in data	2.45E-10	
CHFCl ₂	6.05E-12	1.69E-10		6.52E-10	1.93E-09	
CH ₂ Br ₂	9.61E-08	4.21E-08		4.53E-08	5.28E-08	
CCl ₂ H ₂	low vap. press.	1.75E-10		6.43E-10		
CCl ₃ H	4.68E-09	6.22E-09		1.69E-8		
SiCl ₄	1.56E-08	3.06E-09		5.16E-10		

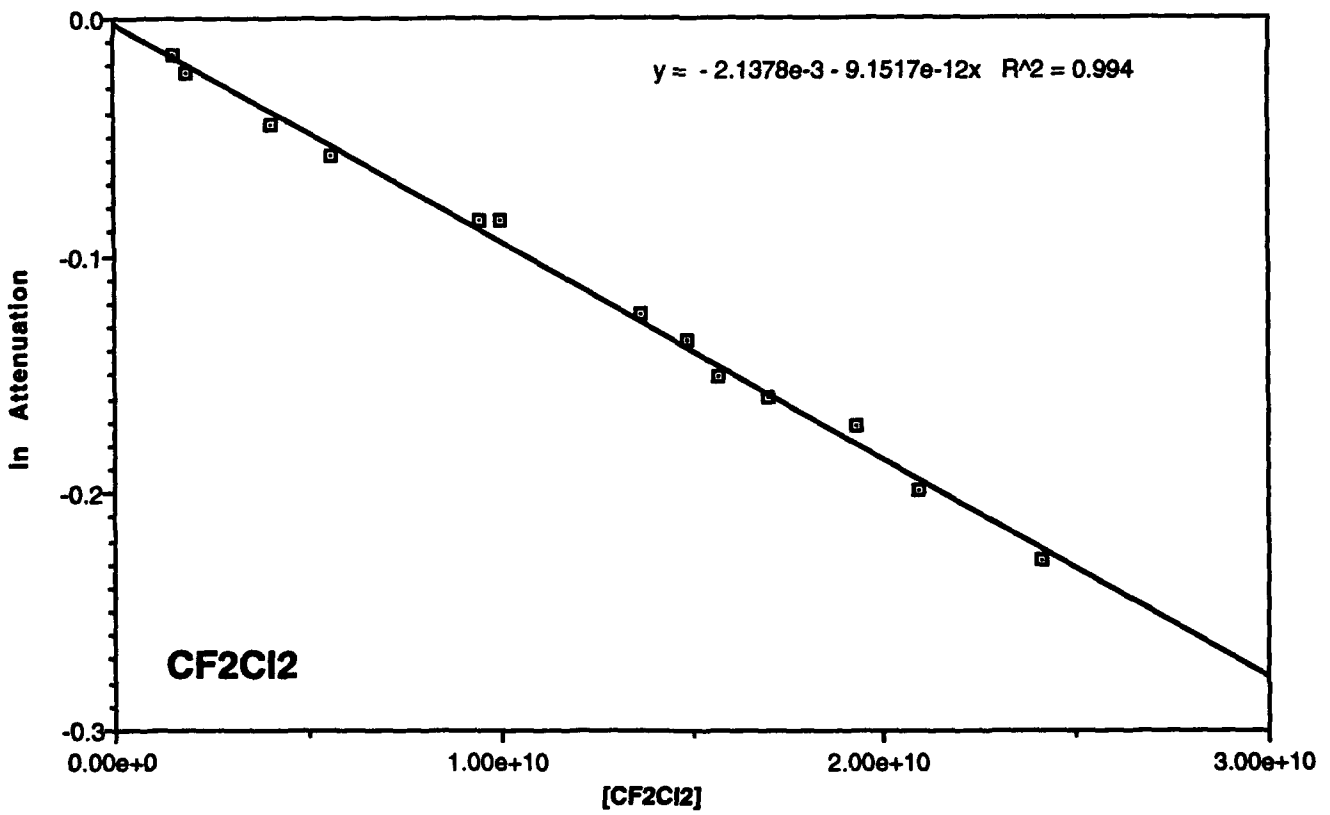
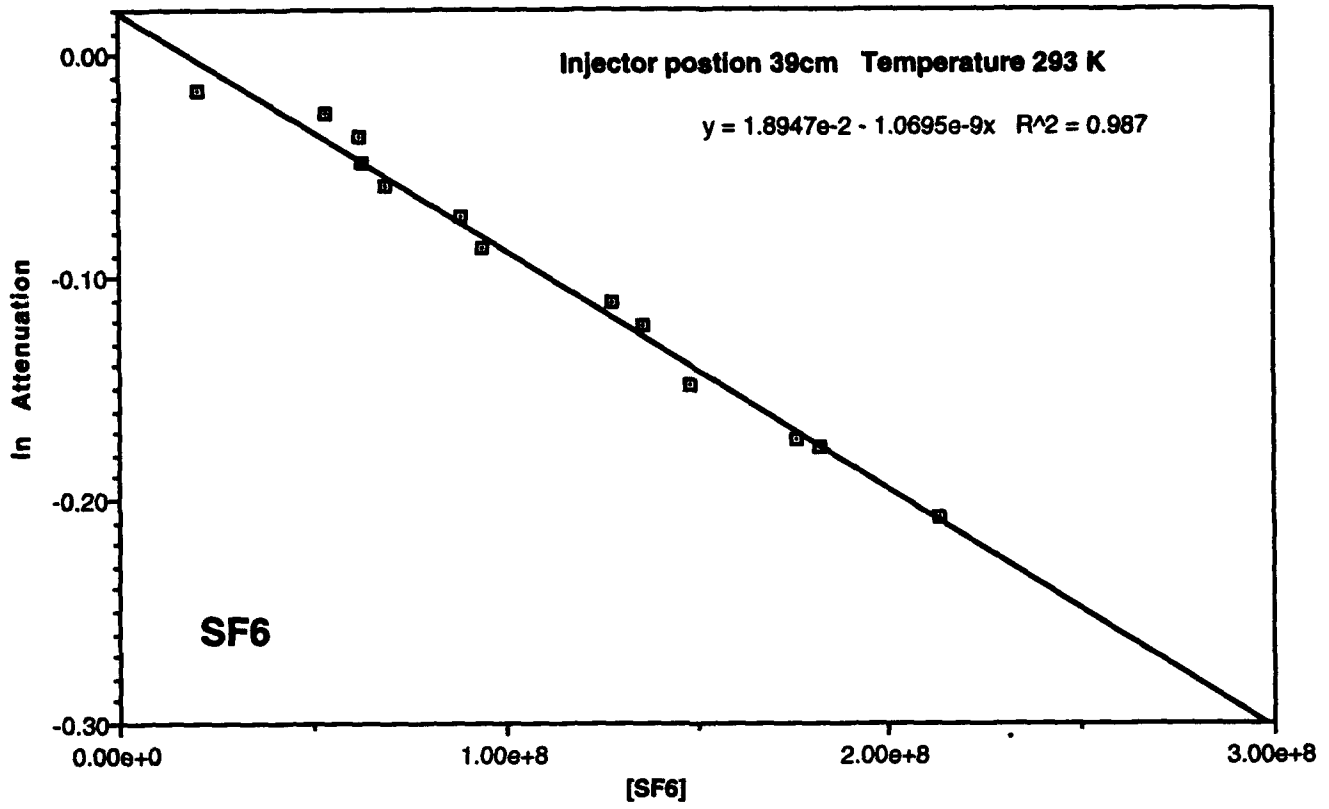


Figure 4

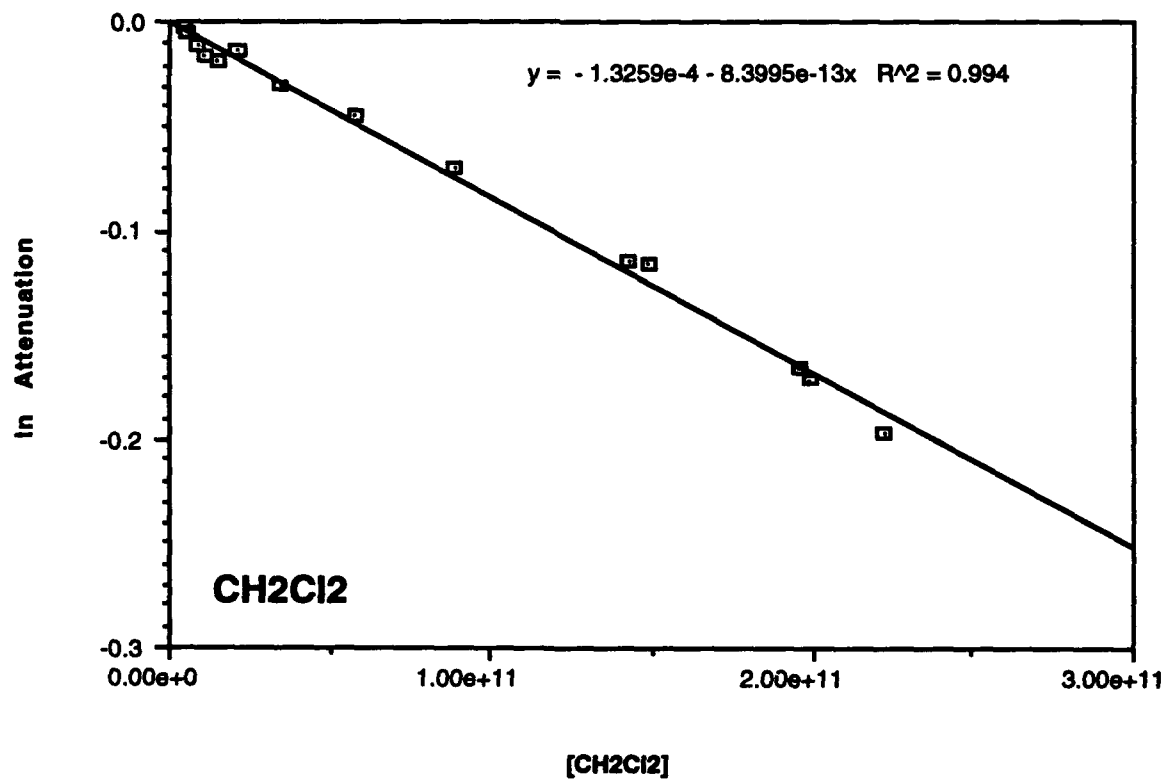
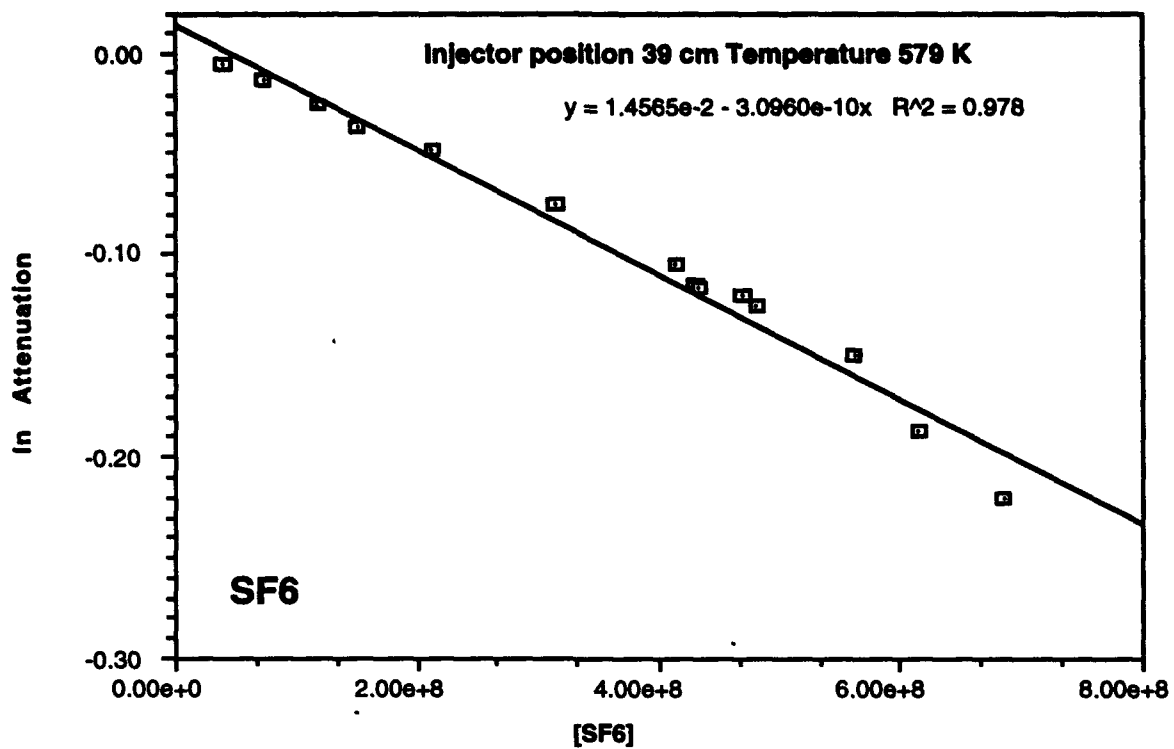


Figure 5

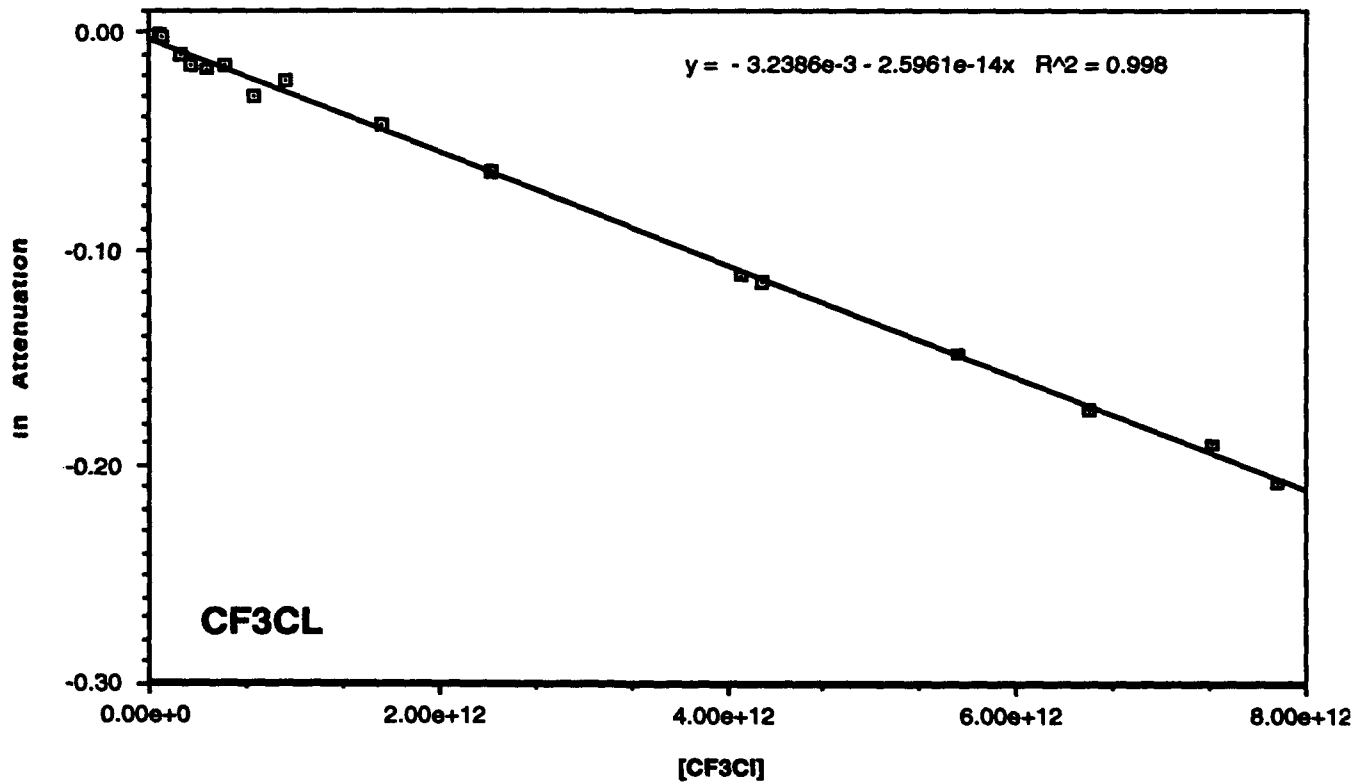
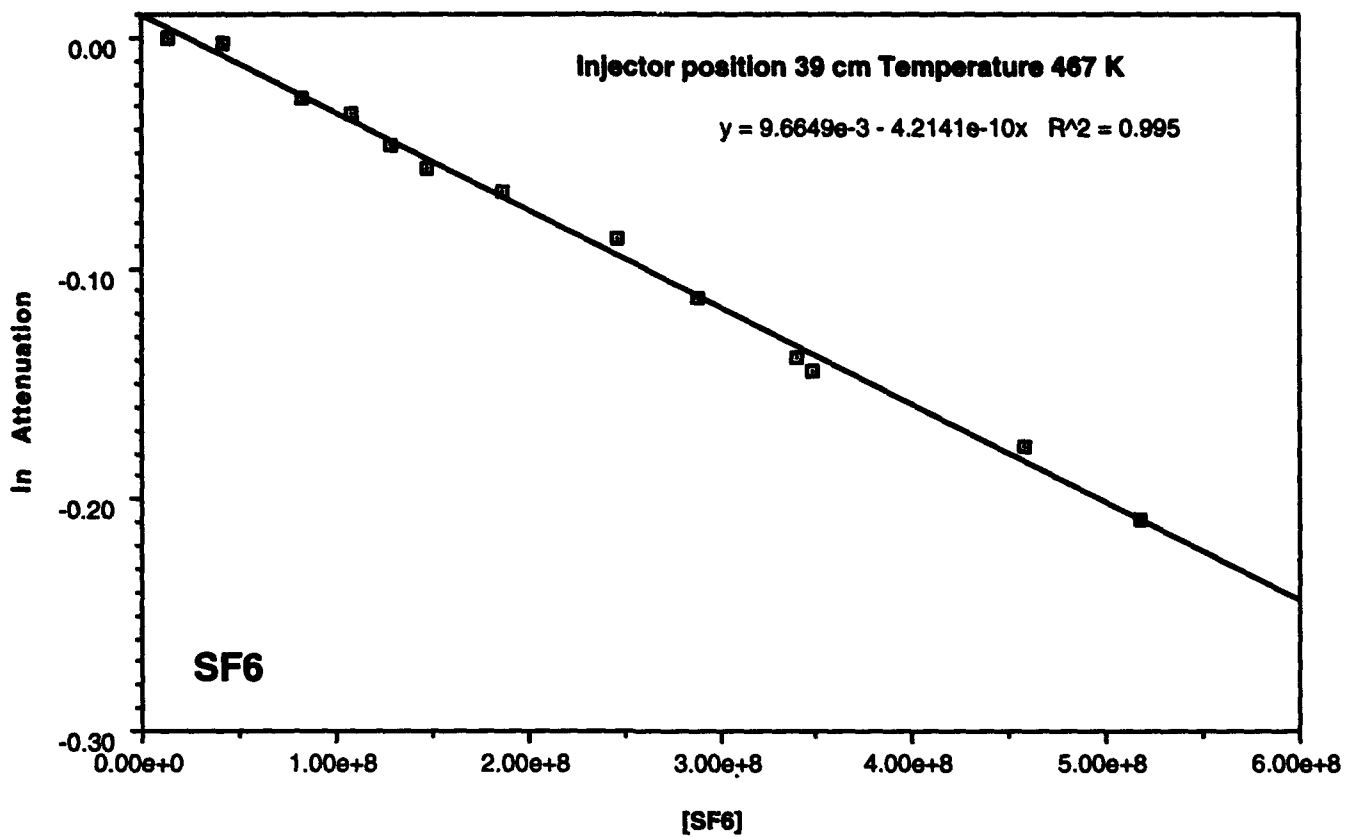


Figure 6

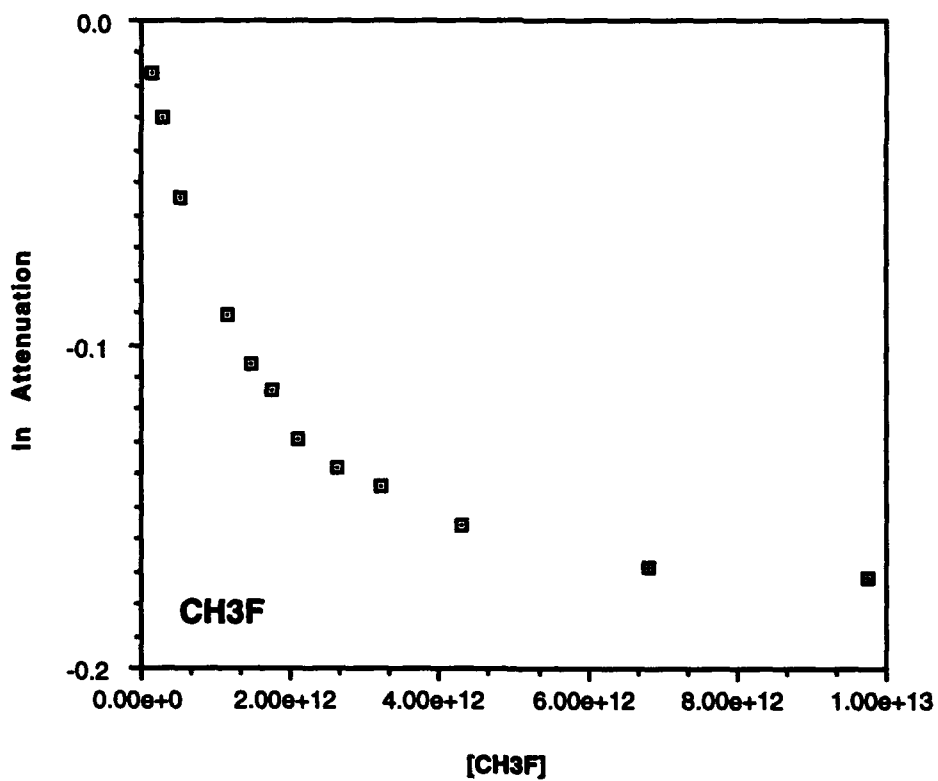
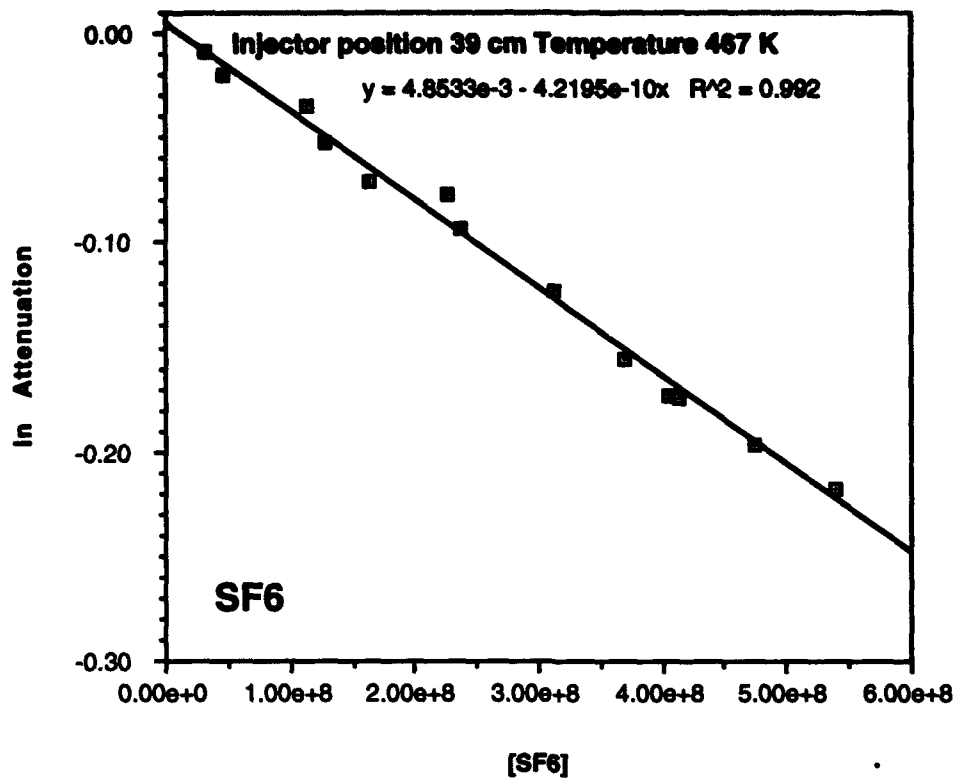


Figure 7

The data from Table 1 are plotted in Figures 8-9 (p. 15). A few of the data points deserve special comment. The measurements indicate that the rate constants for CCl_4 and CH_2Br_2 are somewhat higher at room temperature than at elevated temperatures. Although these numbers may stand up, further checks on these systems are indicated. Compounds such as these, which are liquids at room temperature, are subject to condensation in the storage bulbs and in the transfer lines, leading to incorrect concentration measurements. These data will be rechecked prior to publication. The very steep temperature dependence of the CHFCl_2 rate constant is also unusual and may indicate the presence of an unwanted reaction beginning to participate at high temperature.

Two additional compounds that are not halocarbons, POCl_3 and SiCl_4 , were also investigated, and the results are listed in Table 1 and shown in Figure 10 (p. 16). The negative temperature dependence for POCl_3 is small and may be the result of decomposition of this relatively unstable compound at the higher temperature. SiCl_4 is the one compound that was studied which undergoes non-dissociative electron transfer, and the steep negative temperature dependence is characteristic of non-dissociative electron attachment. High temperature experiments that are needed to complete Table 1 are in progress and will be included in the publication of the complete study.

The results of mass spectral analysis of the anionic reaction products are summarized in Table 2 (p. 17). Regardless of the reaction being studied, there is always a relatively large background of Cl^- in the mass spectrum, so Cl^- as a reaction product is difficult to confirm. In the cases where Cl^- is noted as a major product, it is clearly evident above the background. As expected, most of the reactions proceed with formation of a halide ion as the only detectable product. Four of the compounds, CH_3Cl , CH_3F , CH_2F_2 and CHF_3 appeared to react slowly with electrons at room temperature, as noted in Table 1, but no anionic products were detected, even at sufficiently high reactant concentrations to cause complete attenuation of the electron (ECR) signals. With the exception of CH_3Cl , these reactions are endoergic, so it is not surprising that anionic products were not detected, but it is not clear what is responsible for the attenuation of

Rate Constants vs. Temperature

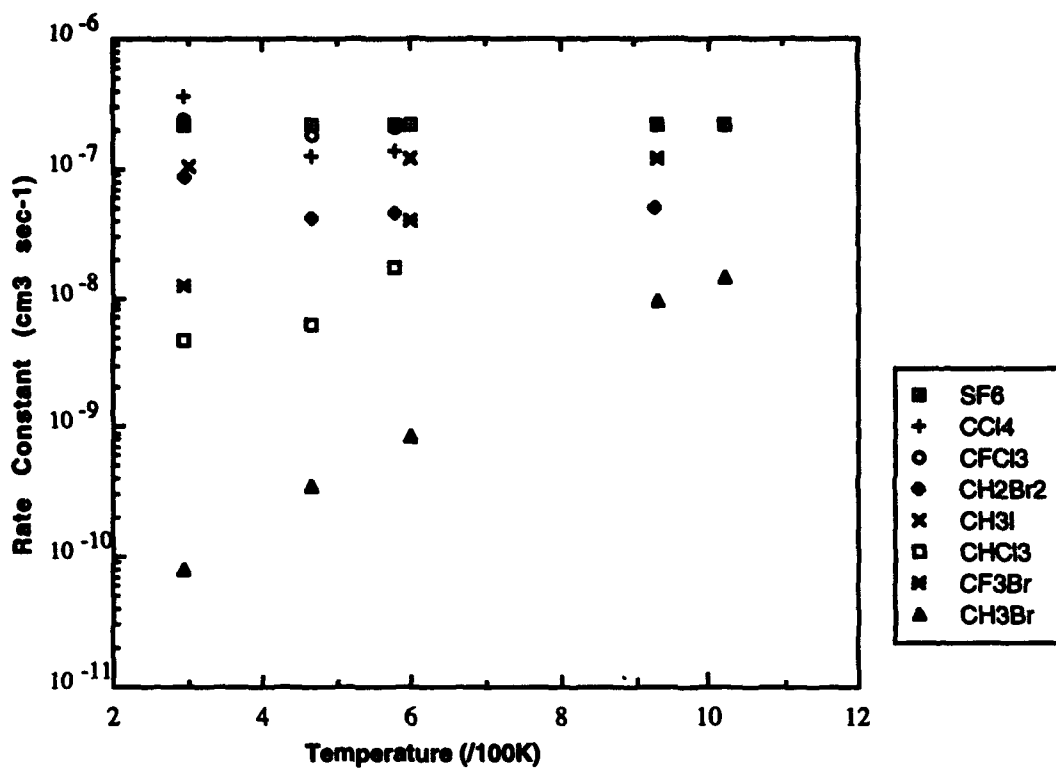


Figure 8

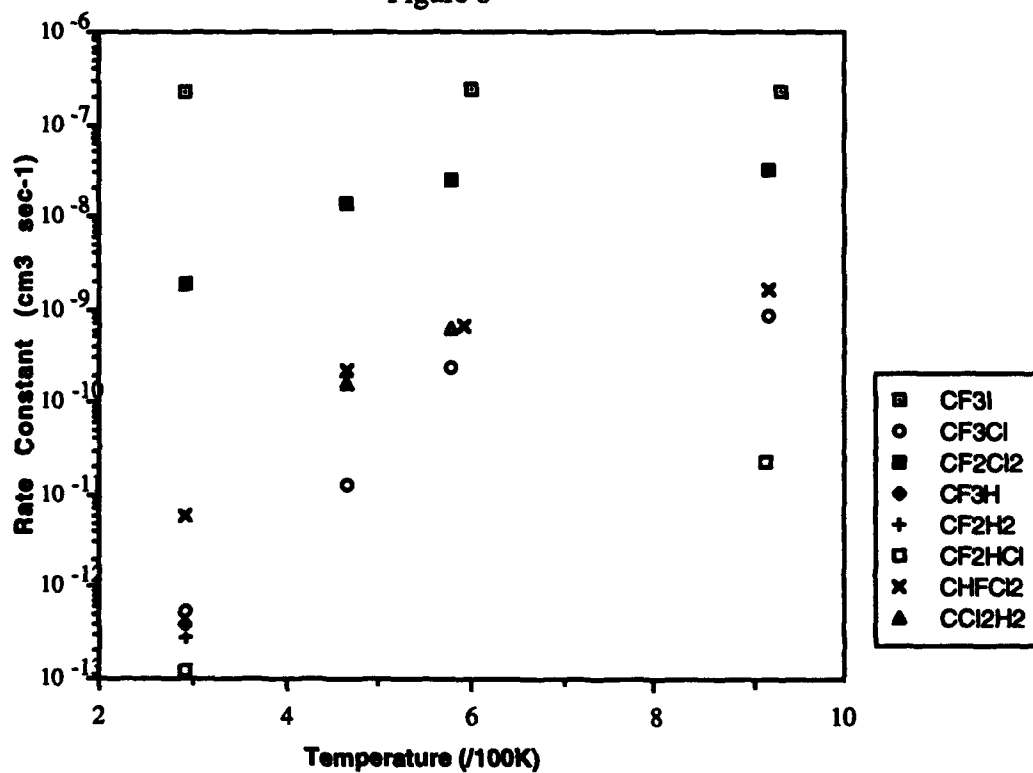


Figure 9

Rate Constants vs Temperature

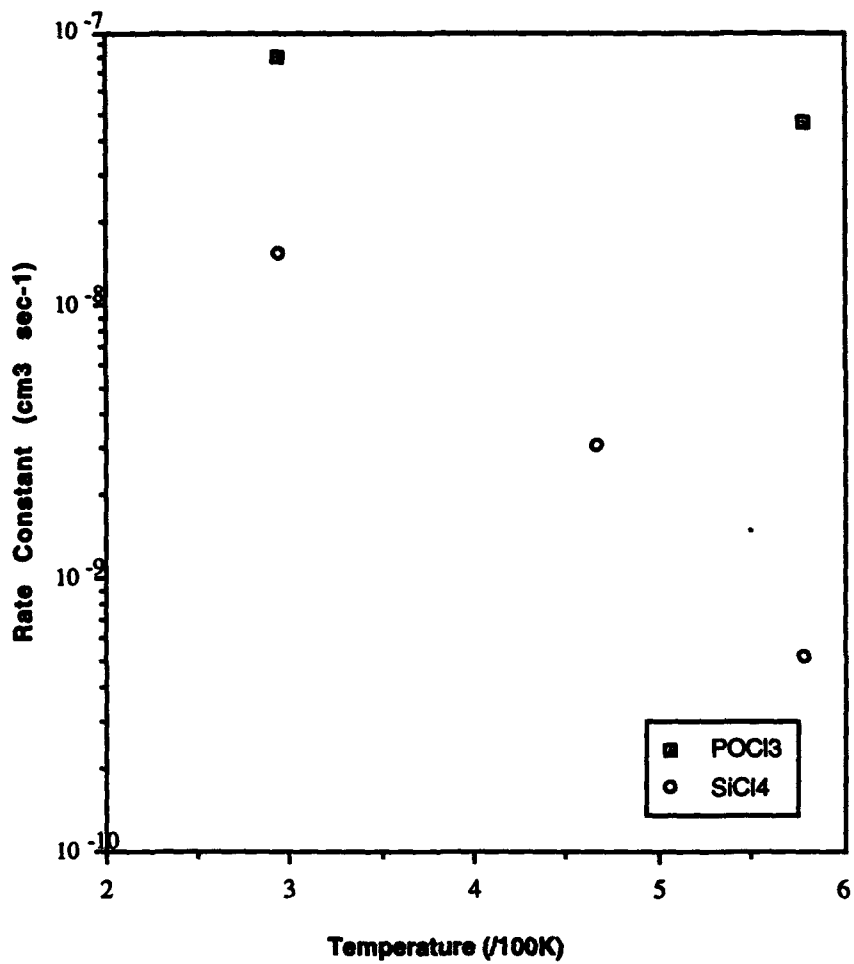


Figure 10

electrons. Products of clustering between Cl^- and the neutral reactant were detected for CHF_2Cl and CHFCl_2 at room temperature and for CF_3H at 579 K. For POCl_3 , both the parent anion and POCl_2^- were observed at room temperature, but the parent anion was missing at elevated temperature. Also, the absence of SiCl_4^- at higher temperature was unexpected. The production of Cl^- in the case of SiCl_4 at elevated temperature is thought to result from wall reactions or from some secondary process.

Table 2. Negative Ion Products of Electron Attachment Reactions

Compound	Temperature		
	293 K	467 K	579 K
	Product Anions Detected		
CH_3I	I^-	I^-	I^-
CH_3Br	Br^-	Br^-	Br^-
CH_3Cl	No products	Cl^-	Cl^-
CF_3I	I^-	I^-	I^-
CF_3Br	Br^-	Br^-	Br^-
CF_3Cl	Cl^-	Cl^-	Cl^-
CF_2Cl_2	Cl^-	Cl^-	Cl^-
CFCl_3	Cl^-	Cl^-	Cl^-
CCl_4	Cl^-	Cl^-	Cl^-
POCl_3	POCl_3^- , POCl_2^-	POCl_2^- , Cl^-	POCl_2^- , Cl^-
CF_3H	No products	sm. F^-	CF_3HCl^-
CF_2H_2	No products	sm. F^- , $\text{H}^-?$	No products
CH_3F	No products	No products	No products
CF_2HCl	$\text{CF}_2\text{HCl}_2^-$	Cl^-	Cl^-
CHFCl_2	$\text{CCl}_2\text{HFCI}^-$	Cl^-	Cl^-
CH_2Br_2	Br^-	Br^-	Br^-
CCl_2H_2	Cl^-	Cl^-	Cl^-
CCl_3H	Cl^-	Cl^-	Cl^-
SiCl_4	SiCl_4^-	$\text{Cl}^-?$	$\text{Cl}^-?$

4. Theoretical Model for Temperature Dependent Rate Constants

In an attempt to model the results of the kinetics experiments, we explored the possibility that geometry differences between the neutral reactant molecule and the ground state negative ion intermediate formed by electron attachment determine the rate constant of the attachment process. According to this view, if the neutral molecule and its anion have essentially identical geometries

(bond lengths and bond angles), then a collision between a free electron and a neutral molecule will, with high probability, lead to dissociative electron attachment. In this case, the rate constant would be equal to the electron-molecule collision frequency, which is determined by the deBroglie wavelength (i.e., size) of the free electron. The greater the difference in molecular geometries at room temperature, the smaller the room temperature attachment rate. The fact that the bond lengths of the anions are in many cases greater than those of the neutral molecules leads to a positive temperature dependence for the attachment rate constant for those molecules. As the temperature is increased, collision-induced vibrational excitation stretches the molecule and creates a larger population of neutral molecules with a geometry identical to the intermediate anion. The higher the frequency (or energy) of the vibrational mode that must be excited to effect the required geometry change, the steeper the temperature dependence is expected to be.

This simple picture was suggested by the results of calculations of the lowest energy geometries for the neutral molecules and for the corresponding negative ions. The calculations were performed on a CAChe computer system by using the MOPAC program, which is based on a semi-empirical quantum mechanical method of calculating molecular geometries and energetics. The geometries obtained from MOPAC include all of the bond lengths and bond angles. The bond lengths that undergo a significant change in the process of electron attachment are shown in Table 3 for each molecule investigated. Experimentally determined geometries for the neutral molecules (bond lengths and bond angles) are also included in Table 3 so that the accuracy of the MOPAC calculations can be evaluated.

The results of these calculations show, for example, that SF₆, which has a very large room temperature rate and no temperature dependence, experiences very little change in geometry in going from a neutral molecule to a stable anion. On the other hand, CH₃Br, which reacts slowly at room temperature and has a positive temperature dependence, shows a significant stretching of the carbon-bromine bond.

**Table 3: MOPAC Geometries for Neutral Molecules and Anions,
Experimental Geometries for Neutral Molecules, and Scaled geometries for Anions**

	Bond or Angle	MOPAC molecule geometries	MOPAC anion geometries	Exper. molecule geometries*	Scaled geometries of anion
SF ₆	S-F	1.54 Å	1.58 Å	1.564 Å	1.608 Å
	F-S-F	90.00°	89.98°	90°	
CCl ₄	C-Cl	1.76 Å	1.82 Å	1.760 Å	1.823 Å
	Cl-C-Cl	109.47°	109.47°	109.47°	
CFCl ₃	C-Cl	1.79 Å	1.88 Å	1.76 Å	1.85 Å
	C-F	1.38 Å	1.36 Å	1.33 Å	
	Cl-C-Cl			109°41'	
	F-C-Cl	110.77°	109.60°	109°28'	
CF ₂ Cl ₂	C-Cl	1.81 Å	1.96 Å	1.77 Å	1.92 Å
	C-F	1.37 Å	1.36 Å	1.33 Å	
	F-C-F	102.50°	101.62°	109.5°	
	Cl-C-Cl			108.5°	
	F-C-Cl	111.97°	110.46°		
CF ₃ Cl	C-F	1.37 Å	1.37 Å	1.328 Å	2.014 Å
	C-Cl	1.82 Å	2.09 Å	1.751 Å	
	F-C-F	105.76°	104.58°	108.6°	
	F-C-Cl	113.01°	114.02°	110.33°	
CH ₃ Cl	C-H	1.11 Å	1.09 Å	1.0959 Å	2.7187 Å
	C-Cl	1.74 Å	2.66 Å	1.7812 Å	
	H-C-H	110.62°	119.44°	108°	
	H-C-Cl	108.30°	85.02°	110°55'	
CH ₃ Br	C-H	1.11 Å	1.10 Å	1.113 Å [†]	2.207 Å
	C-Br	1.90 Å	2.17 Å	1.939 Å [†]	
	H-C-H	110.15°	113.32°	111°14' [†]	
	H-C-Br	108.78°	105.32°		
CH ₃ I	C-H	1.11 Å	1.10 Å	1.113 Å [†]	2.3138 Å
	C-I	2.05 Å	2.22 Å	2.1392 Å [†]	
	H-C-H	109.83°	111.89°	111°25' [†]	
	H-C-I	109.08°	107.00°		
CF ₃ Br	C-F	1.37 Å	1.37 Å	1.328 Å	2.059 Å
	C-Br	2.04 Å	2.20 Å	1.909 Å	
	F-C-F	104.89°	102.74°	108.6°	
	F-C-Br	113.74°	115.58°	110.33°	
CF ₃ I	C-F	1.37 Å	1.38 Å	1.332 Å	2.2606 Å
	C-I	2.18 Å	2.31 Å	2.130 Å	
	F-C-F	104.48°	102.07°	108.3°	
	F-C-I	114.09°	116.11°	110.62°	
CF ₃ H	C-F	1.37 Å	1.38 Å	1.333 Å	1.333 Å
	C-H	1.13 Å	1.37 Å	1.098 Å	
	F-C-F			108.6°	
	F-C-H	113.03°	115.23°	110.33°	
CF ₂ H ₂	C-F	1.37 Å	1.38 Å	1.358 Å	1.336 Å
	C-H	1.13 Å	1.38 Å, ₁	1.092 Å	
	F-C-F	103.93°		108°17'	
	H-C-H		106.80°	111°52'	
	H-C-F	110.44°	107.13°		

	Bond or Angle	MOPAC molecule geometries	MOPAC anion geometries	Exper. molecule geometries*	Scaled geometries of anion
CH ₃ F	C-H	1.12 Å	1.39 Å, ¹	1.095 Å	1.362 Å
	C-F	1.38 Å	1.38 Å	1.391 Å	
	H-C-H	109.49°	104.65°	109.5°	
	H-C-F	109.45°	122.09°		
CF ₂ HCl	C-H	1.13 Å	1.11 Å	1.09 Å	2.68 Å
	C-Cl	1.81 Å	2.16 Å	1.74 Å	
	C-F	1.37 Å	1.36 Å	1.35 Å	
	H-C-Cl			107°	
	Cl-C-F	112.45°	113.25°	110.5°	
	F-C-F	103.19°	104.39°	107°	
	F-C-H	111.91°	112.55°		
CFHCl ₂	C-H	1.12 Å	1.12 Å	1.09 Å	1.89 Å
	C-Cl	1.78 Å	1.92 Å	1.75 Å	
	C-F	1.37174 Å	1.36173 Å	1.367 Å	
	Cl-C-Cl			112°12'	
	F-C-Cl	111.89°	111.35°	109°	
	H-C-Cl			109°45'	
	F-H-H	110.21°	109.92°		
CH ₂ Br ₂	C-H	1.11 Å	1.10 Å		
	C-Br	1.90 Å	2.01 Å		
	H-C-H	110.28°	112.78°		
	H-C-Br	108.23°	104.81°		
CH ₂ Cl ₂	C-H	1.11 Å	1.10 Å	1.068 Å	1.9080 Å
	C-Cl	1.74 Å	1.87 Å	1.7724 Å	
	H-C-H	112.18°	113.93°	112°	
	H-C-Cl	107.95°	104.05°		
	Cl-C-Cl			111.8°	
CHCl ₃	C-H	1.11 Å	1.11 Å	1.100 Å	1.834 Å
	C-Cl	1.75 Å	1.82 Å	1.758 Å	
	H-C-Cl	107.67°	103.98°	107°34'	
	Cl-C-Cl			111°18'	

*All values obtained from reference [3] unless otherwise noted.

†Reference [4]

Although the calculated geometry change, which is based on equilibrium bond distances, is small for a molecule such as SF₆ that exhibits no temperature dependence, there is still a change. Such small changes, however, fall within the average displacement from the equilibrium position defined by the root mean square deviation and therefore are considered insignificant:

$$\langle x^2 \rangle^{1/2} = \left\{ \left(\nu + \frac{1}{2} \right) \left(\frac{\hbar}{2\pi c \bar{\nu}_{\text{obs}} \mu} \right) \right\}^{1/2} \quad (1)$$

where v is the vibrational quantum number, $\hbar = 1.05459 \times 10^{-34}$ J s, $c = 3.00 \times 10^8$ m s⁻¹, $\bar{\nu}_{\text{obs}}$ is the observed vibrational frequency in units of m⁻¹, and μ is the reduced mass in units of kg [5]. Assuming that the molecules behave as harmonic oscillators, calculations show that the root mean square deviation from equilibrium of SF₆ is equal to the change in geometry of the SF₆ molecule that results from attachment of an electron. Table 4 shows the results of several such calculations. Therefore, on the average, SF₆ molecules at room temperature attain the same geometry as the anions prior to encountering an electron. It is this condition that appears to be necessary for highly efficient attachment. Since this is true for SF₆ at all temperatures, this model would predict the absence of a temperature dependence, which Schulz showed to be the case up to 1500 K.

Table 4: Comparison of Critical Stretching (x_c) to the Root Mean Square Deviation from Equilibrium (rmsd) at Different Vibrational Levels

Compound	x_c , Å	Vibr'l. Level	rmsd, Å
SF ₆	0.044	0	0.0426865
CCl ₄	0.063	0	0.0638083
CFCl ₃	0.09	0	0.0855559
CF ₂ Cl ₂	0.15	0	0.0497663
		4	0.149299
CF ₃ Cl	0.263	0	0.0389549
		23	0.267061
CH ₃ Cl	0.9375	0	0.0466852
		25	0.333399
CH ₃ Br	0.268	0	0.0466782
		16	0.268146
CH ₃ I	0.1746	0	0.0484984
		6	0.174864
CF ₃ Br	0.1500	0	0.036157
		8	0.149079
CF ₃ I	0.1306	0	0.0364281
		6	0.131343
CF ₃ H	0.235	0	0.0772605
		5	0.256244
CF ₂ H ₂	0.244	0	0.0760388
		5	0.252192

Compound	x_c , Å	Vibr'l. Level	rmsd, Å
CH ₃ F	0.267	0	0.0781672
		6	0.281836
CF ₂ HCl	0.34	0	0.0450564
		25	0.321767
CFHCl ₂	0.14	0	0.052163
		3	0.13801
CH ₂ Br ₂	0.10378*	0	0.0456642
		2	0.10378
CH ₂ Cl ₂	0.1356	0	0.047024
		4	0.141072
CHCl ₃	0.076	0	0.0525485
		1	0.0910166

This value is based on MOPAC calculations rather than experimental data.

Other molecules, however, seem to require a change in their room temperature geometry before attachment of an electron can lead to product formation. In many cases, such as CH₃Br, this primarily involves the stretching of only one bond. Such stretching can result from vibrational excitation of the relevant mode at elevated temperatures.

Our initial approach to modeling the temperature dependence of the rate constants is to calculate, as a function of temperature, the probability (or the fraction of time) that the relevant bond in the neutral molecule is stretched to a length equal to or greater than the calculated bond length in the stable anionic intermediate.

4.1. Calculations

The first step in calculating the temperature dependence of the required geometry change is to determine the most important vibrational mode of the neutral molecule that, if excited, leads to the geometry of the anion. The extent of stretching that is required is also determined. This is done by evaluating the MOPAC geometries for both the neutral molecule and the parent anion. The data in Table 3 show that, for the molecules under investigation, there is primarily one bond that stretches as a result of electron attachment, while the other bonds do not change significantly. Also, the changes in bond angles are small and probably do not involve significant energy changes

as compared to the stretching of bonds. The bond which experiences the greatest change in length following electron attachment is identified. The vibrational mode of the neutral molecule that is responsible for this stretching is then identified. This is the vibrational mode of interest. The extent of stretching required for electron attachment is calculated by subtracting the bond length in the neutral molecule from the bond length in the anion. Experimental bond lengths are used for the neutral molecules, and the MOPAC results for the neutrals are compared with the experimental values to obtain a scaling factor that is applied to the MOPAC bond lengths for the anions. The difference in bond lengths is referred to as x_c , the critical stretching. Tables 3 and 4 summarize these results. Table 5 shows information needed to carry out these calculations.

Table 5: Values Required to Carry Out Calculation of Rate Constants

Compound	2-Body Harmonic Oscillator	Bond Stretched	Vibr'l. Mode of Interest*	Obs. vib. freq. [†] , cm ⁻¹	Scaled vib. freq. of anion, cm ⁻¹
SF ₆	F-F	S-F	ν_1	775 [‡]	756
CCl ₄	C-Cl	C-Cl	$\nu_1(a_1)$	461.5 [‡]	372
CFCl ₃	C-Cl	C-Cl	$\nu_1(a_1)$	349.5	256.7
CF ₂ Cl ₂	CF ₂ -Cl	C-Cl	$\nu_9(b_2)$	446	327.9
CF ₃ Cl	CF ₃ -Cl	C-Cl	$\nu_3(a_1)$	474	315.4
CH ₃ Cl	CH ₃ -Cl	C-Cl	$\nu_3(a_1)$	732.1 [‡]	124.3
CH ₃ Br	CH ₃ -Br	C-Br	$\nu_3(a_1)$	611 [‡]	374.94
CH ₃ I	CH ₃ -I	C-I	$\nu_3(a_1)$	532.8 [‡]	366.5
CF ₃ Br	CF ₃ -Br	C-Br	$\nu_3(a_1)$	348	267
CF ₃ I	CF ₃ -I	C-I	$\nu_3(a_1)$	284	211
CF ₃ H	C-H	C-H	$\nu_1(a_1)$	3035	1569
CF ₂ H ₂	CF ₂ -H	C-H	$\nu_1(a_1)$	2949	1524
CH ₃ F	C-H	C-H	$\nu_1(a_1)$	2965	1439
CF ₂ HCl	CF ₂ -Cl	C-Cl	$\nu_9(b_2)$	400	204
CHFCl ₂	CFH-Cl	C-Cl	$\nu_9(b_2)$	368	217

Compound	2-Body Harmonic Oscillator	Bond Stretched	Vibr'l. Mode of Interest*	Obs. vib. freq.†, cm ⁻¹	Scaled vib. freq. of anion, cm ⁻¹
CH ₂ Br ₂	CH ₂ -Br	C-Br	v ₉ (b ₂)	677.05††	416.34††
CH ₂ Cl ₂	CH ₂ -Cl	C-Cl	v ₉ (b ₂)	758	442
CHCl ₃	C-Cl	C-Cl	v ₂ (a ₁)	680	525

*Vibrational modes were identified using reference [6].

†Observed vibrational frequencies were obtained from reference [3] unless otherwise noted.

‡Reference [6]

††This value was obtained by scaling the MOPAC frequency.

The second step is to calculate the probability that the bond is stretched by the amount x_c as a function of the vibrational quantum number, v . The known or calculated vibrational frequency for the desired vibrational mode is used and harmonic oscillator wave functions are assumed. The probability is calculated as follows:

$$P_{x_c}(v) = \int_{x_c}^{\infty} \Psi_v^2 dx \quad (2)$$

$$= \frac{1}{\pi^{1/2} 2^v v!} \int_{x_c/\alpha}^{\infty} H_v^2(y) e^{-y^2} dy \quad (3)$$

where x_c is the critical stretching of the molecule, Ψ_v is the wave function of a harmonic oscillator, $\alpha = (\hbar^2/\mu k)^{1/4}$, $k = (2\pi c \bar{\nu}_{obs})^2 \mu$ in units of kg/s², and $H_v(y)$ is a Hermite polynomial. Table 6 lists the Hermite polynomials [7].

Table 6: The Hermite Polynomials*

The first seven Hermite polynomials, $H_v(y)$, are as follows:

v	$H_v(y)$
0	1
1	$2y$
2	$4y^2 - 2$
3	$8y^3 - 12y$
4	$16y^4 - 48y^2 + 12$
5	$32y^5 - 160y^3 + 120y$
6	$64y^6 - 480y^4 + 720y^2 - 120$

The Hermite polynomials (which continue up to infinite v) satisfy the equation

$$H_v'' - 2yH_v' + 2vH_v = 0$$

and the recursion relation

$$H_{v+1} = 2yH_v - 2vH_{v-1}.$$

An important integral is

$$\int_{-\infty}^{\infty} e^{-y^2} H_v H_{v'} dy \begin{cases} = 0 & \text{if } v' \neq v \\ = \pi^{1/2} 2^v v! & \text{if } v' = v. \end{cases}$$

*The information in this table is taken from reference [7], p. 324.

Third, the probability of populating a particular vibrational level v as a function of temperature is calculated as follows:

$$P_v(T) = \frac{e^{-E_v/k_B T}}{\sum_v e^{-E_v/k_B T}} \quad (4)$$

where $E_v = (v + 1/2)h\nu$, $\nu = (k/\mu)^{1/2}$ in units of s^{-1} , and k_B is Boltzmann's constant.

Finally, the probability that the molecule is stretched by the necessary amount as a function of temperature is given by:

$$P_{x_c}(T) = \sum_v P_{x_c}(v) P_v(T) \quad (5)$$

The calculation of $P_{x_c}(T)$ was carried out by using *Mathematica* software on a Macintosh IIfx computer. Calculations for *rmsd*, reduced masses, alpha, omega, and *xctp-anion* required, on the

average, less than a minute to complete. The $P_{x_c}(T)$ and $P_{x_{ctp}}(T)$ calculations took approximately 10 minutes each.

The temperature dependent rate constant, $k(T)$, can then be related to the theoretical maximum rate constant, k_{max} , by an expression involving this probability:

$$k(T) = k_{max} P_{x_c}(T) \quad (6)$$

The calculation of $k(T)$ was carried out at five different temperatures: 300, 600, 900, 1200, and 2000 K. The value of k_{max} , which is determined by the deBroglie wavelength of the electron [8], is also temperature dependent:

$$k_{max} = \frac{h^2}{(2\pi)^{3/2} m^{3/2} (k_B T)^{1/2}} \quad (7)$$

where $h = 6.62618 \times 10^{-34}$ J s, $m_e = 9.10953 \times 10^{-31}$ kg, $k_B = 1.38066 \times 10^{-23}$ J K⁻¹, and T is the temperature in Kelvin. The values of k_{max} at selected temperatures are given in Table 7.

Table 7: Maximum Rate Constant as a Function of Temperature

Temperature, K	k_{max} , cm ³ /s
300	4.9821×10^{-7}
600	3.5229×10^{-7}
900	2.8764×10^{-7}
1200	2.4911×10^{-7}

The assumption made for the calculations, that the required bond stretch is from the equilibrium separation for the neutral molecule to the equilibrium separation for the anion, is an arbitrary one. In order to test how sensitive the calculations are to x_c , calculations were also carried out by using the left classical turning point of the ground vibrational level of the anion instead of the equilibrium separation to determine x_c . This value was designated x_{ctp} .

4.2. Results and Discussion

Typical results of the calculations are shown in Figure 11 (p. 29) for the case where the relevant bond in the neutral molecule is stretched by an amount x_c , the difference in the equilibrium bond lengths between the neutral and the anion. The calculated values display the same type of temperature dependence as the experimental rate constants as well as the broad range of values for the room temperature rate constants. This is illustrated for two molecules, CH_3Br and CFCl_3 , in Figure 12 (p. 30), where the experimental rate constants are plotted together with the calculated values for the two different limits of stretching, x_c and x_{ctp} . There are large quantitative differences, particularly at the lower temperatures, between the two calculated values, but for most of the molecules studied, the experimental values fall within the range defined by the two calculated values. Figures 13-14 (p. 31) shows a comparison of the experimental rate constants with the two sets of calculated room temperature rate constants (at room temperature the difference between the two calculated values is the largest). Between the two sets of calculated values, better agreement with experiment is shown in Figure 13, which gives the results for stretching the neutral molecule to the classical turning point of the anion. Figure 14 gives the results for the case of stretching the neutral molecule by the larger amount, x_c , corresponding to the difference in equilibrium bond lengths between the neutral molecule and the anion. Clearly, the calculations are very sensitive to the amount of stretching that is specified within this crude model. The experimental rate constants vary over seven orders of magnitude, and the calculated values reflect this broad range. Of more importance than the actual numbers, however, is the order of the molecules from slowest to fastest, which the calculations do not reproduce exactly. Of the twelve molecules listed, four are out of order. Two of them are iodide compounds, CH_3I and CF_3I . The iodide compounds react more rapidly, by factors of 4 and 7, respectively, than indicated by the calculated values. It is possible that the MOPAC program is less accurate for the case of the heavy iodide compounds and that either the increase in bond length in the anion is overestimated or the vibrational frequencies are inaccurate. The other two compounds, which are even more out of line, are CHCl_3 and CF_2Cl_2 .

For these molecules the experimental rate constants are 50 and 10 times smaller, respectively, than the calculated values. The experimental values are believed to be reliable. Comparison of our room temperature rate constants with those from other laboratories is good.

The results of the calculations indicate that this simple model is a reasonable starting point and seem to confirm that a significant mismatch between the geometries of the neutral molecule and the anion does lead to a very small rate constant for dissociative electron attachment, despite the absence of an energy barrier in these exoergic reactions. The calculations do not give the correct order, however, for some of the faster reactions, indicating perhaps that while the geometry does play a role, other factors not included in the model may also be important.

The model suggests that electron attachment leads to dissociation and product formation only if there is a relatively large Franck-Condon overlap between the neutral molecule and intermediate anion. When there is a substantial geometrical mismatch between the two species, an electron-molecule collision is non-reactive, and the electron is ejected from the anionic intermediate before the energetically favored dissociation products have a chance to separate. Viewing the reaction in this way suggests that, instead of calculating the probability of stretching a bond by some critical amount, perhaps one ought to calculate the Franck-Condon overlap between the two sets of wavefunctions as a function of temperature. The Franck-Condon overlap formula for two harmonic oscillators of different frequencies and different internuclear separations is available in the literature [9], and this formulation of the model will be tested in the near future.

Further improvement in the model might also result from using more accurate potential functions that include the addition of an anharmonic term. This would have the effect of putting more curvature in the plots, which would increase the agreement between the model and experimental results.

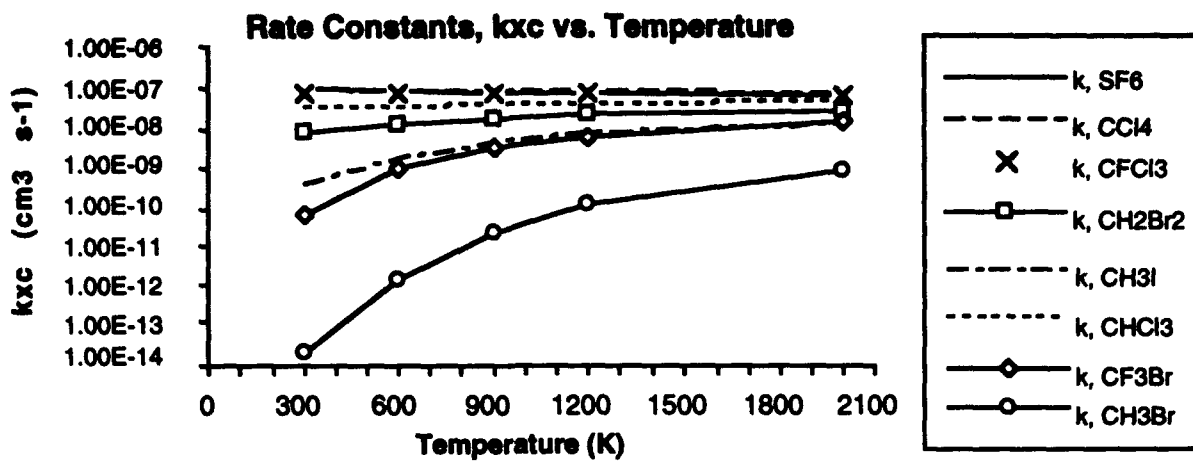


Figure 11

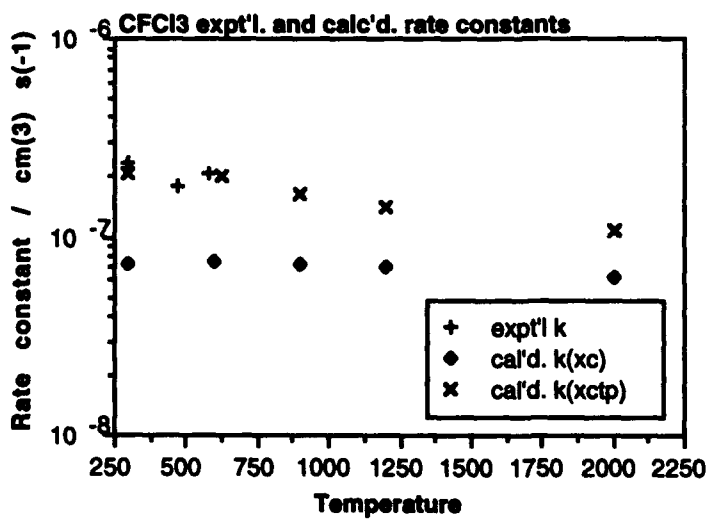
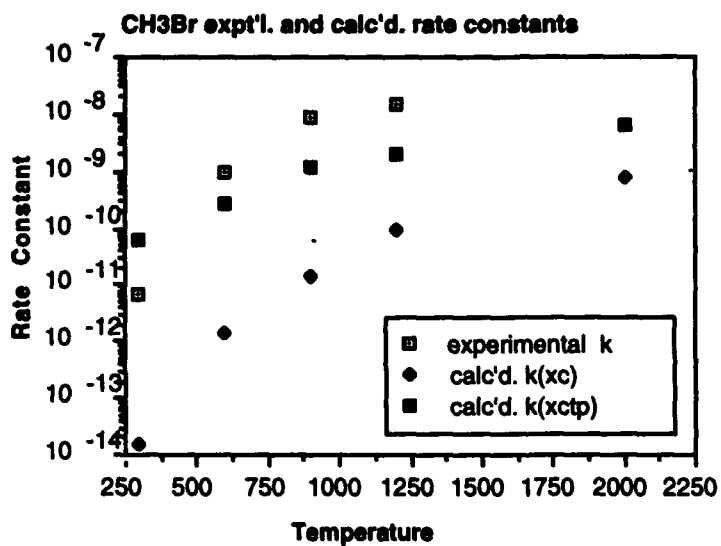


Figure 12

Comparison of experimental and calculated rate constants

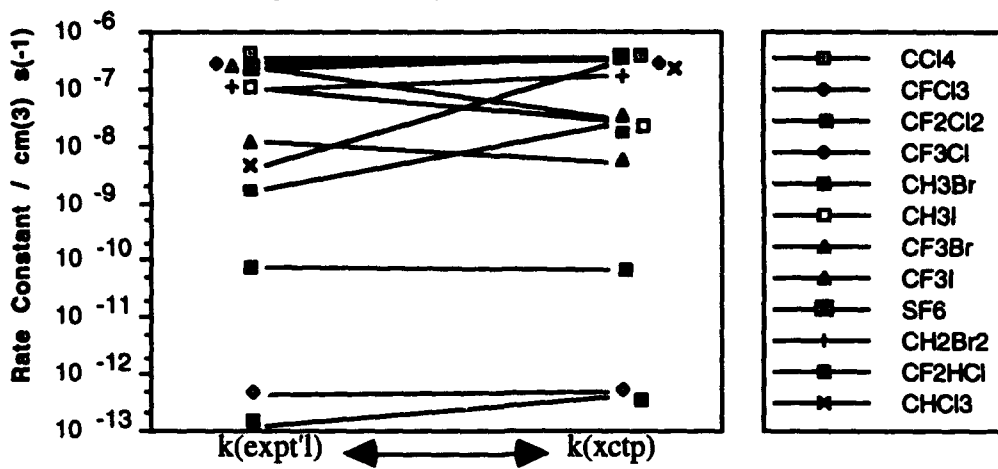


Figure 13

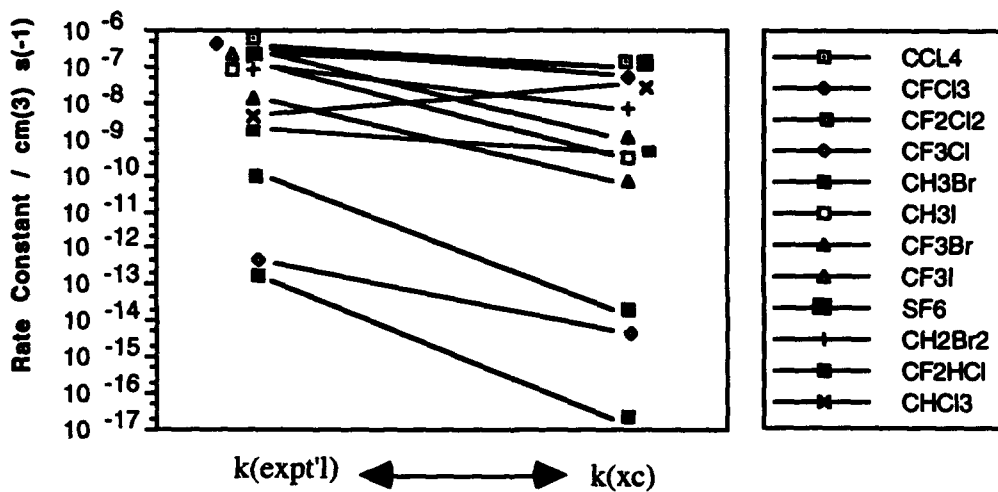


Figure 14

References

- (1) Spence, D. and Schulz, G. J., Journal of Chemical Physics, **58**, 1800 (1972).
- (2) Petrovic, Z. Lj., and Crompton, R. W., Journal of Physics B: Atomic and Molecular Physics **18**, 2777 (1985).
- (3) JANAF Thermochemical Tables, Third Edition, Journal of Physical and Chemical Reference Data, **14**, 1985, Suppl. 1.
- (4) Townes, C. H. and Schalow, A. L., *Microwave Spectroscopy*, (Dover Publication, Inc. New York, 1975).
- (5) McQuarrie, D. A., *Quantum Chemistry*, University Science Books, Mill Valley, CA, 1983.
- (6) Herzberg, G., *Molecular Spectra and Molecular Structure: Infrared and Raman Spectra of Polyatomic Molecules*, Van Nostrand Reinhold Company, NY, 1945.
- (7) Atkins, P. W., *Physical Chemistry*, Third Ed., W.H. Freeman and Co., NY, 1986.
- (8) Warman, J. M. and Sauer, M. C., Jr., International Journal of Radiation Physics and Chemistry, **3**, 273-282 (1971).
- (9) Beddard, G. S., Fleming, G. R., Gijzeman, O. L. J. and Porter, G., Chemical Physics Letters, **18**, 481 (1973).

Articles to be published from this research

Determination of Rate Constants for Thermal Electron Attachment Reactions of CH₃Br, CF₃Br, and CF₃I over the Temperature Range $300 \leq T(K) \leq 1100$, Robert G. Levy, Steven J. Burns and David L. McFadden, *Chem. Phys. Lett.* (to be submitted).

Temperature Dependence of Dissociative Electron Attachment Rate Constants for Reactions of Thermal Energy Electrons and Halomethanes, Steven J. Burns, Jeanne M. Matthews and David L. McFadden, *J. Chem. Phys.* (to be submitted).

Thermal Energy Electron Attachment Reaction of POCl₃, Steven J. Burns and David L. McFadden, *Chem. Phys. Lett.* (to be submitted).

Thermal Energy Electron Attachment Reaction of SiCl₄, Jeanne M. Matthews, Steven J. Burns and David L. McFadden, *Chem. Phys. Lett.* (to be submitted).